Amyloid Formation

Zitierweise:
Internationale Ausgabe: doi.org/10.1002/anie.202113845
Deutsche Ausgabe: doi.org/10.1002/ange.202113845

Inhibitor-Mediated Structural Transition in a Minimal Amyloid Model

*Priyadarshi Chakraborty, Santu Bera, Phil Mickel, Ashim Paul, Linda J. W. Shimon, Zohar A. Arnon, Daniel Segal, Petr Král, and Ehud Gazit**

Abstract: *Despite the fundamental clinical importance of amyloid fibril formation, its mechanism is still enigmatic. Crystallography of minimal amyloid models was a milestone in the understanding of the architecture and biological activities of amyloid fibers. However, the crystal structure of ultimate dipeptide-based amyloids is not yet reported. Herein, we present the crystal structure of a typical amyloid-forming minimal dipeptide, Ac-Phe-Phe-NH_2 (Ac-FF-NH_2), showing a canonical β-sheet structure at the atomic level. The simplicity of the structure helped in investigating amyloid-inhibition using crystallography, never previously reported for larger peptide models. Interestingly, in the presence of an inhibitor, the supramolecular packing of Ac-FF-NH_2 molecules rearranged into a supramolecular 2-fold helix (2_1 helix). This study promotes our understanding of the mechanism of amyloid formation and of the structural transitions that occur during the inhibition process in a most fundamental model.*

Amyloid fibril formation, which occurs due to the aggregation of proteins and polypeptides, is associated with various diseases with unrelated aetiologies, including Alzheimer's disease, Parkinson's disease, amyotrophic lateral sclerosis, Huntington's disease, Creutzfeldt–Jakob disease, and type II diabetes.[1] Amyloids exhibit distinctive common characteristics, including Thioflavin T binding, Congo red birefringence, and high content of ordered β-strands.[2–4] Deciphering the mechanism of amyloid formation is of utmost importance for the study and discovery of novel therapeutic directions to hinder this process.[5–7]

One of the most insightful and accurate tools to unravel the structural basis for biological activity is crystallography. Indeed, in the case of amyloids, the structure of the cross-β spine of amyloid fibrils was deduced from the microcrystal of a seven-residue peptide segment of the yeast protein, Sup35.[8] Furthermore, the structures of other segments from fibril-forming proteins were determined including Alzheimer's Amyloid-beta (Aβ) and tau proteins, the PrP prion protein, insulin, islet amyloid polypeptide (IAPP), lysozyme, myoglobin, α-synuclein and β_2-microglobulin.[9] Additionally, microcrystal structures of eight different fibril-forming segments of the Aβ peptide, including the $A\beta_{16\text{-}21}$ (^{16}KLVFFA^{21}) segment, exhibited self-complementing pairs of β-sheets termed steric zippers.[10] These pioneering studies by Eisenberg and co-workers demonstrate that amyloid diseases share some common structural characteristics at the molecular level, which can be revealed by short peptides models. The picture was later revealed to be more complicated as some amyloid assemblies were recently reported to form cross-α organization as well.[11,12] The molecular basis for the occurrence of either cross-α or cross-β organization and the transition between the two is still enigmatic.

We have previously identified the diphenylalanine (FF) dipeptide as the core recognition motif of the Aβ peptide that undergoes self-assembly into ordered structures showing high resemblance to amyloid structures.[13] This reductionist approach is based on our hypothesis that the energetic contribution as well as the assembly order and directionality of the well-ordered amyloid nanostructures stem from stacking interactions, rather than hydrophobicity. The key role for aromatic interactions in the self-assembly process of amyloid nanostructures is supported by the very simple structure of the FF dipeptide. However, it is difficult to rule out the possibility of electrostatic interactions in the self-assembly process of FF, as it is comprised of two opposing charges on both its termini, an amine at the N-terminus and a carboxyl at the C-terminus. There is a genuine unmet need to elucidate the crystal structure of the minimal amyloid-forming building block.

Herein, we adopted a reductionist approach in order to unravel the major factors responsible for protein aggregation (Figure 1). To this end, we explored the self-assembly mechanism of the non-charged peptide Ac-FF-NH_2, the

[*] Dr. P. Chakraborty, Dr. S. Bera, Dr. A. Paul, Dr. Z. A. Arnon, Prof. D. Segal, Prof. E. Gazit
Shmunis School of Biomedicine and Cancer Research
George S. Wise Faculty of Life Sciences
Tel Aviv University
Tel Aviv 6997801 (Israel)
E-mail: ehudg@post.tau.ac.il

P. Mickel
Department of Chemistry
University of Illinois at Chicago
845 West Taylor St, Chicago, IL 60607 (USA)

Prof. P. Král
Departments of Chemistry, Physics, Pharmaceutical Sciences, and Chemical Engineering
University of Illinois at Chicago
845 West Taylor St, Chicago, IL 60607 (USA)

L. J. W. Shimon
Department of Chemical Research Support,
Weizmann Institute of Science, Rehovot 76100 (Israel)

Prof. E. Gazit
Department of Materials Science and Engineering
Iby and Aladar Fleischman Faculty of Engineering
Tel Aviv University
Tel Aviv 6997801 (Israel)

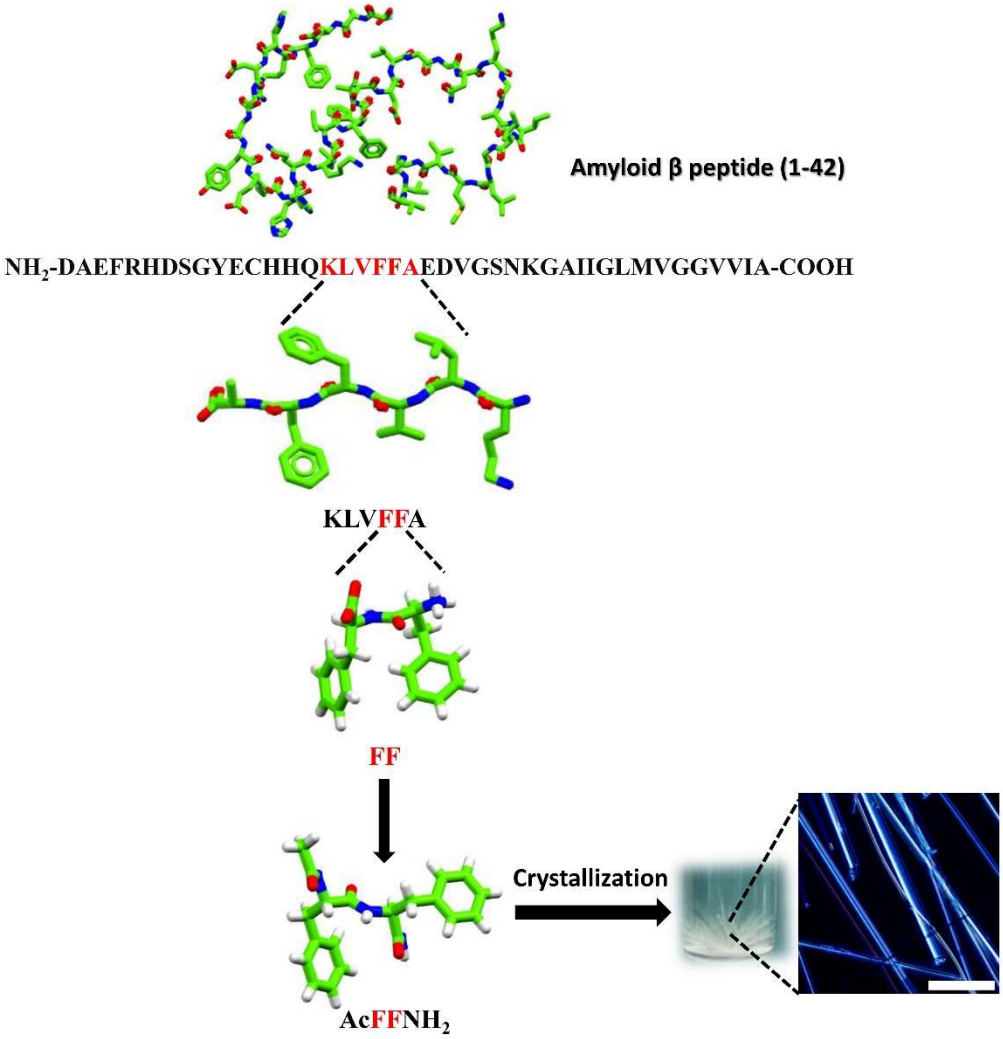

Figure 1. A reductionist model showing the crystallization of Ac-FF-NH_2 into needle-shaped crystals. The microscopy image shows crystals under polarized light. Scale bar: 100 μm.

simplest building block known to form amyloid-like fibrils, via crystallization.[14] We also set out to investigate the effect of amyloid modulators on the crystal structure of Ac-FF-NH_2. Since rosmarinic acid (RA) was previously observed to be a very potent inhibitor and a destabilizer of the amyloid aggregates obtained from FF,[15] we used this compound to investigate the modulation of the molecular arrangement of Ac-FF-NH_2 at the atomic level and higher order packing.

Colourless crystals of the dipeptide suitable for X-ray diffraction (XRD) studies were obtained from methanol–water solutions (9:1) by slow evaporation (Figure S1).[16] The crystals were needle shaped (Figure S1a) and exhibited blue luminescence (Figure S1b). The amyloidogenic nature of the crystals was examined using a thioflavin-T (ThT) binding assay, an amyloid-specific fluorescent dye (Figure S1d). Upon staining the crystals with ThT, high fluorescence levels were observed, along with a typical amyloid binding emission signal, thus establishing their amyloidogenic nature. We then studied the effect of RA on the amyloid structure formation of Ac-FF-NH_2 by monitoring the ThT fluorescence over time (Figure S2). For Ac-FF-NH_2 alone, ThT fluorescence increased rapidly and reached a plateau within 500 min. However, lower ThT fluorescence signal was observed in the presence of RA, signifying the inhibition of amyloid-like aggregate formation by Ac-FF-NH_2. The conformation and molecular organization of the Ac-FF-NH_2 dipeptide was further studied at the atomic level using single crystal XRD. The dipeptide crystalized in monoclinic, polar space group $P2_1$ with one molecule in the asymmetric unit (Figure 2a, S3 & Table S1). X-ray structure analysis revealed the two aromatic side chains are organized in opposite directions with respect to the peptide backbone. Torsion angles around the phenylalanine moieties played a pivotal role in determining the overall molecular conformation. The important backbone torsion angles of the dipeptide are listed in Table S2. The individual molecules of Ac-FF-NH_2 pack along a two-fold screw aligned along the crystallographic *b*-axis. The overall packing is stabilized

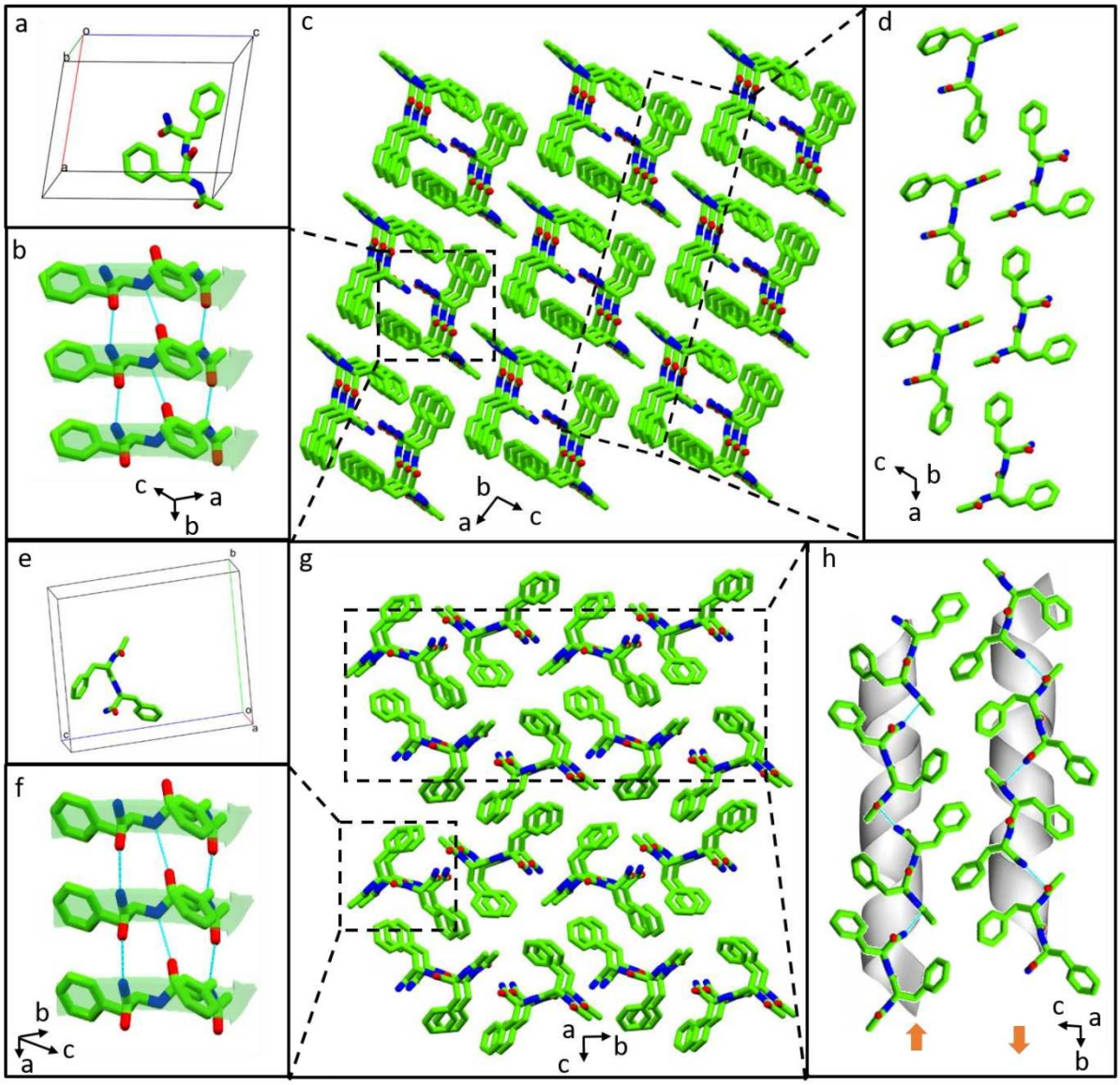

Figure 2. Single crystal structure of Ac-FF-NH_2 prepared (a–d) in the absence of an inhibitor and (e–h) in the presence of RA. a–d) Pure Ac-FF-NH_2 structure: a) the asymmetric unit, b) β-sheet arrangement stabilized through H-bonds and π–π interactions, c) higher order packing demonstrating the formation of cage-like architectures through dimeric aggregation, and d) the interfacial stabilization of the cages. e–h) Ac-FF-NH_2 structure in the presence of RA: e) the asymmetric unit, f) β-sheet arrangement of molecular units, g) higher order packing showing a layer-by-layer arrangement which is significantly different to that of pure Ac-FF-NH_2 crystal structure (compare to panel c), and h) supramolecular helical-like organization of the individual layer formed through head-to-tail H-bonds between molecular units in the crystallographic *b*-direction. Heteroatoms nitrogen and oxygen are represented in blue and red, respectively. H-bonds are shown in dotted cyan line. For clear visualization, peptide structures in b, f and h are superimposed over ideal β-sheet and helical models.

through three intermolecular hydrogen bonds, N1–H1···O1, N2–H2···O2 and N3–H3B···O3 (Table S3), as well as two aromatic–aromatic interactions (centroid-centroid distances of 4.908 Å) (Figure 2b & S3). The resulting structure generates a supramolecular parallel β-sheet organization of the molecular units.[17] Two series of adjacent sheets were stabilized through van der Waals interactions and afforded a cage-like cyclic packing (Figure 2c). Distribution of such cage-like architectures bound through hydrophobic interactions built the higher order supramolecular packing of Ac-FF-NH_2 (Figure 2d). This crystal packing is completely different from the *syn* arrangement of aromatic side chains identified in the structure of unprotected, nanotube-forming NH_2-FF-COOH, which contains hydrogen-bonded head-to-tail chains in the shape of helices and gives rise to a hydrophilic channel.[18] Due to the absence of any intra-

molecular H-bonds, the packing of Ac-FF-NH_2 was also found to be significantly different from the reported inverse γ-turn structure-forming protected diphenylalanine, Boc-FF-OMe,[19] as well as from other amyloid forming diphenylalanine derivatives, Fmoc-FF-COOH, Boc-FF-COOH and Cbz-FF-COOH.[20,21]

To understand the modulation of molecular arrangement at the atomic level and the higher order packing due to incorporation of the inhibitor, diffraction-quality single crystals of the dipeptide were grown from a methanol–water solution in the presence of RA.[22–24] Under the modified circumstances, Ac-FF-NH_2 crystallized with one molecule in an asymmetric unit in orthorhombic space group, $P2_12_12_1$ (Figure 2e, S4 & Table S1). The torsion angles for the Phe_1 and Phe_2 residues showed alteration values due to presence of RA as compared to the pure peptide crystal (Table S2). Individual subunits stacked through three intermolecular H-bonding interactions (N1–H1···O1, N2–H2···O2 and N3–H3B···O3) and two π–π stacking interactions (shortest centroid–centroid distance 4.857 & 4.974 Å) and produced parallel β-sheet structure in the crystallographic *a*-direction (Figure 2f, S4 & Table S3). However, a significant modulation of the higher order packing was induced by the presence of the inhibitor. The differences in the packing pattern of crystal growth in the absence and presence of the RA inhibitor can be well identified in Figure 2c and g. Stabilization through head-to-tail H-bonding (N3–H3A···O1) between the molecular units was prompted due to presence of RA during the crystallizing process, generating a one-dimensional columnar array along the crystallographic *b*-axis (Figure 2g, h & S4). Although the torsion angle around the Phe_1 residue did not reflect affinity to bend into a helical structure, a supramolecular 2-fold helix (2_1 helix) could be evidently recognized by considering the molecular shapes around the specific helical axis (*b*-axis).[25,26] Two adjacent helical sheets were oriented in antiparallel fashion and stabilized through hydrophobic interactions of aromatic rings which formed an "aromatic zipper" like structural arrangement at the molecular interface. These results show that the change in the supramolecular packing of inhibited Ac-FF-NH_2 at the atomic level likely restricts the macroscopic long-range alignment of the crystal, growing one-dimensionally into the observed fibrils. To date, studies on the inhibition effect of the aggregation process of different proteins and peptides has been based on conventional methods such as transmission electron microscopy (TEM), Fourier-transform infrared spectroscopy (FTIR), and circular dichroism (CD), while understanding the mechanism of such events is solely dependent on molecular dynamics simulation prediction.[24,27] However, the finer structural details at the atomic level still remain elusive. To the best of our knowledge, the current results reveal, for the first time, the inhibitor-mediated structural modulation of a short amyloid-forming model peptide at the atomic level providing crucial insights regarding the underlying mechanism of the inhibition process.

To determine how the presence of the inhibitor affects the crystal growth, we performed atomistic molecular dynamics simulations of the RA and Ac-FF-NH_2 molecules adsorbed on the facets of Ac-FF-NH_2 crystals in the methanol–water solution (9:1) and compared their free energies of binding to the crystal surfaces, calculated by the MMGB-SA method (see Supporting Information for details). Two different Ac-FF-NH_2 crystals were used in the simulations: 1) (native) crystals experimentally observed to form alone and 2) (inhibited) crystals experimentally observed to form in the presence of RA molecules. To understand why the native crystals grow alone, we have separately calculated the free energies of binding of the Ac-FF-NH_2 molecules embedded in the top facets of both crystals.

Figures 3a,b and c,d show RA molecules adsorbed on the native and inhibited Ac-FF-NH_2 crystals in the methanol–water solution, respectively. Figures 3a,c show the planes of the fastest crystal growth, whereas in Figures 3b,d the crystals are rotated forward. Figure 3e shows the calculated free energies of binding of the RA and Ac-FF-NH_2 molecules to the 6 facets of each chiral crystal (see Supporting Information). The free energy of binding between the RA molecules and the native crystal was larger in magnitude than that between the Ac-FF-NH_2 molecules and this crystal, suggesting that the native crystal does not grow in the presence of RA molecules, which are outcompeting the Ac-FF-NH_2 molecules for surface adsorption. This is particularly clear in the crystal growth facets (dark blue, orange). However, the free energy of binding between the RA molecules and the inhibited crystal was lower in magnitude than that between the Ac-FF-NH_2 molecules and this crystal, indicating that the inhibited crystal grows in the presence of the RA molecules, which are outcompeted by the Ac-FF-NH_2 molecules for surface adsorption.

Figure 3f also shows that the average free energy of binding of the (embedded) Ac-FF-NH_2 molecules was larger for the native than the inhibited crystals, indicating that native crystals should grow in the absence of RA molecules. In total, the simulation results reveal why the native crystals are formed in the absence of RA molecules, while the inhibited crystals are formed in their presence.

In order to extend our observation that supramolecular packing of amyloid-forming dipeptides rearranges at the atomic level in the presence of inhibitors, we further studied the effect of RA on the aggregation propensity, conformational changes and structure of the hexapeptide KLVFFA, the major driver for Aβ aggregation in Alzheimer's disease, and Aβ42, the major causative peptide in Alzheimer's disease (Figure S5, S6, Supporting note S1). Amyloid formation by KLVFFA and Aβ42 in the presence of different molar ratios of RA was monitored by ThT binding assay and showed a decrease of ThT fluorescence in a dose-dependent manner indicating inhibition of amyloid formation. CD spectroscopy similarly revealed a decrease in β-sheet content of KLVFFA and Aβ42 in the presence of RA. TEM images revealed elongated dense fibrillar morphology for both KLVFFA and Aβ42 aggregates. However, in the presence of RA, fibril density was markedly reduced in a dose-dependent manner. We further performed powder XRD analysis of the amyloid aggregates in both the

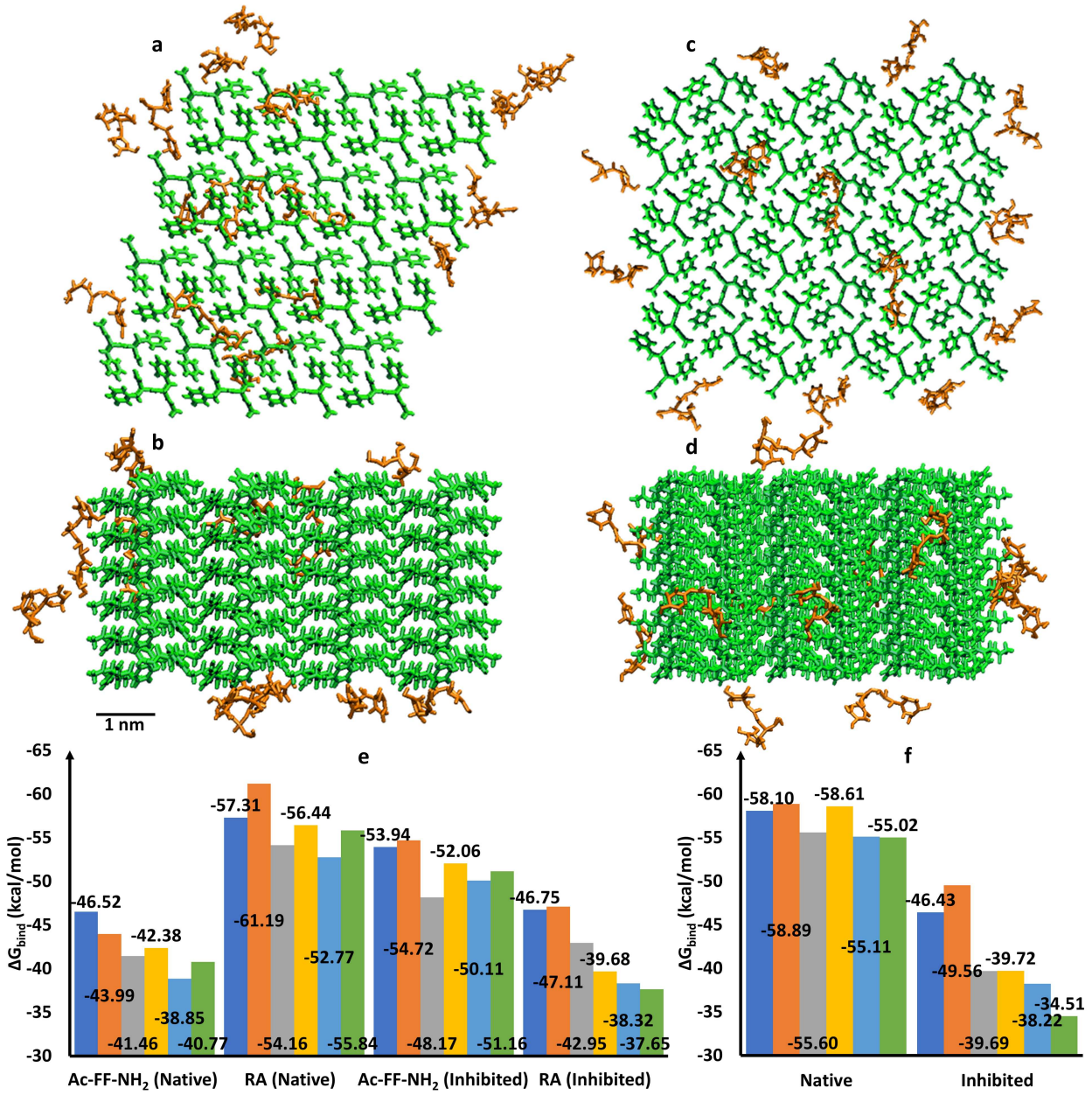

Figure 3. Atomistic molecular dynamics simulations of RA adsorbed on different Ac-FF-NH_2 crystal facets. a) Top and b) side views of the native Ac-FF-NH_2 crystal with several RA molecules on its surface. c) Top and d) side views of the inhibited Ac-FF-NH_2 crystal. e) The free energies of binding of individual RA and Ac-FF-NH_2 molecules to the native and inhibited Ac-FF-NH_2 crystals, normalized for the number of attached molecules. f) Free energies of binding of the Ac-FF-NH_2 molecules within each of the 6 facets of the native and inhibited Ac-FF-NH_2 crystals, normalized for the number of molecules in each facet. From left to right, columns represent (1 0 0), (−1 0 0), (0 1 0), (0 −1 0), (0 0 1), and (0 0 −1) facets. The crystals were aligned such that their growth facets were aligned with the same indices.

presence and absence of RA to decipher the structural changes (Figure S7,8). The sharp peaks exhibited by the KLVFFA aggregates appeared to be absent in the powder XRD patterns in the presence of RA (Figure S7), indicating a change in the long-range order of the aggregates. Likewise, the peaks corresponding to β-sheet distance and inter-strand spacing (at 10.8 and 4.4 Å, respectively) in the powder XRD pattern of Aβ42 aggregates[9,28,29] diminished in intensity in the presence of RA (Figure S8), signifying the change in the long-range order. These studies corroborated our reductionist model depicting the effect of inhibitors on the supramolecular packing of amyloid aggregates.

In conclusion, we report, for the first time, the crystal structure of a minimal amyloid-forming peptide, Ac-FF-NH_2. The dipeptide formed needle-like, colourless crystals with blue fluorescence, which could bind to ThT. The crystal structure of the dipeptide revealed a supramolecular parallel β-sheet organization of the molecular units. The crystal packing was markedly different from the structure of unprotected nanotube-forming NH_2-FF-COOH. Intrigu-

ingly, in the presence of the amyloid inhibitor RA, the crystal structure of the dipeptide had substantial alteration of higher order packing. Molecular dynamics also supported the modulation of the higher order packing of the molecules in the presence of RA. Similarly, the higher order packing of the hexapeptide KLVFFA and of the Aβ42 peptide exhibited changes in the long-range order of the amyloid aggregates, validating our reductionist approach. This study exemplifies the inhibitor-mediated structural modulation of short amyloid-forming model peptides and lays the foundation for deciphering the underlying mechanism of amyloid inhibition processes.

Associated Content

Supporting Information. Materials and methods, experimental details, Processing and structural refinement of crystal data, data collection and refinement statistics, important backbone torsion angles of dipeptides, Molecular dynamics (MD) simulations, Inhibition studies of KLVFFA and Aβ42 fibril formation by RA.

Acknowledgement

P.C. gratefully acknowledges Tel Aviv University for financial support and thanks the members of the Gazit laboratory for helpful discussions. The authors thank Sigal Rencus-Lazar for linguistic editing and the members of the Gazit laboratory for helpful discussions. This work was partially supported by grants from the European Research Council under the European Union's Horizon 2020 research and innovation program (BISON, Advanced ERC grant, no. 694426) (E.G.).

Conflict of Interest

The authors declare no conflict of interest.

Keywords: Amyloid fibril · Crystallization · Dipeptide · Inhibitors · β-Sheet

[1] T. P. J. Knowles, M. Vendruscolo, C. M. Dobson, *Nat. Rev. Mol. Cell Biol.* **2014**, *15*, 384–396.
[2] M. Biancalana, S. Koide, *Biochim. Biophys. Acta Proteins Proteomics* **2010**, *1804*, 1405–1412.
[3] R. N. Rambaran, L. C. Serpell, *Prion* **2008**, *2*, 112–117.
[4] T. Eichner, S. E. Radford, *Mol. Cell* **2011**, *43*, 8–18.
[5] B. E. Roberts, J. Shorter, *Nat. Struct. Mol. Biol.* **2008**, *15*, 544–546.
[6] G. M. Shankar, S. Li, T. H. Mehta, A. Garcia-Munoz, N. E. Shepardson, I. Smith, F. M. Brett, M. A. Farrell, M. J. Rowan, C. A. Lemere, C. M. Regan, D. M. Walsh, B. L. Sabatini, D. J. Selkoe, *Nat. Med.* **2008**, *14*, 837–842.
[7] J. Adamcik, J.-M. Jung, J. Flakowski, P. De, L. Rios, G. Dietler, R. Mezzenga, *Nat. Nanotechnol.* **2010**, *5*, 423–428.
[8] R. Nelson, M. R. Sawaya, M. Balbirnie, A. Ø. Madsen, C. Riekel, R. Grothe, D. Eisenberg, *Nature* **2005**, *435*, 773–778.
[9] M. R. Sawaya, S. Sambashivan, R. Nelson, M. I. Ivanova, S. A. Sievers, M. I. Apostol, M. J. Thompson, M. Balbirnie, J. J. W. Wiltzius, H. T. McFarlane, A. Ø. Madsen, C. Riekel, D. Eisenberg, *Nature* **2007**, *447*, 453–457.
[10] J.-P. Colletier, A. Laganowsky, M. Landau, M. Zhao, A. B. Soriaga, L. Goldschmidt, D. Flot, D. Cascio, M. R. Sawaya, D. Eisenberg, *Proc. Natl. Acad. Sci. USA* **2011**, *108*, 16938–16943.
[11] E. Tayeb-Fligelman, O. Tabachnikov, A. Moshe, O. Goldshmidt-Tran, M. R. Sawaya, N. Coquelle, J.-P. Colletier, M. Landau, *Science* **2017**, *355*, 831–833.
[12] M. Landau, *Nat. Chem. Biol.* **2018**, *14*, 833–834.
[13] M. Reches, E. Gazit, *Science* **2003**, *300*, 625–627.
[14] M. Reches, E. Gazit, *Isr. J. Chem.* **2005**, *45*, 363–371.
[15] S. Brahmachari, Z. A. Arnon, A. Frydman-Marom, E. Gazit, L. Adler-Abramovich, *ACS Nano* **2017**, *11*, 5960–5969.
[16] Deposition Numbers 2076137 (for pure Ac-FF-NH_2), and 2076138 (for Ac-FF-NH_2 grown in the presence of RA) contain the supplementary crystallographic data for this paper. These data are provided free of charge by the joint Cambridge Crystallographic Data Centre and Fachinformationszentrum Karlsruhe Access Structures service www.ccdc.cam.ac.uk/structures.
[17] S. K. Maji, L. Wang, J. Greenwald, R. Riek, *FEBS Lett.* **2009**, *583*, 2610–2617.
[18] C. H. Görbitz, *Chem. Eur. J.* **2001**, *7*, 5153–5159.
[19] S. Bera, P. Jana, S. K. Maity, D. Haldar, *Cryst. Growth Des.* **2014**, *14*, 1032–1038.
[20] A. M. Smith, R. J. Williams, C. Tang, P. Coppo, R. F. Collins, M. L. Turner, A. Saiani, R. V. Ulijn, *Adv. Mater.* **2008**, *20*, 37–41.
[21] P. Tamamis, L. A. Abramovich, M. Reches, K. Marshall, P. Sikorski, L. Serpell, E. Gazit, G. Archontis, *Biophys. J.* **2009**, *96*, 5020–5029.
[22] Y. Porat, A. Abramowitz, E. Gazit, *Chem. Biol. Drug Des.* **2006**, *67*, 27–37.
[23] Q. Wang, J. Guo, P. Jiao, H. Liu, X. Yao, *PLoS One* **2014**, *9*, e94796.
[24] S. Brahmachari, A. Paul, D. Segal, E. Gazit, *Future Med. Chem.* **2017**, *9*, 797–810.
[25] I. Hisaki, T. Sasaki, K. Sakaguchi, W.-T. Liu, N. Tohnai, M. Miyata, *Chem. Commun.* **2012**, *48*, 2219–2221.
[26] J. Liang, A. Hao, P. Xing, Y. Zhao, *ACS Nano* **2021**, *15*, 5322–5332.
[27] J. Lu, Q. Cao, C. Wang, J. Zheng, F. Luo, J. Xie, Y. Li, X. Ma, L. He, D. Eisenberg, J. Nowick, L. Jiang, D. Li, *Front. Mol. Neurosci.* **2019**, *12*, 54.
[28] O. Makin, E. Atkins, P. Sikorski, J. Johansson, L. C. Serpell, *Proc. Natl. Acad. Sci. USA* **2005**, *102*, 315–320.
[29] J. C. Stroud, C. Liu, P. K. Teng, D. Eisenberg, *Proc. Natl. Acad. Sci. USA* **2012**, *109*, 7717–7722.

Manuscript received: October 12, 2021
Accepted manuscript online: November 17, 2021
Version of record online: ■■, ■■

Zuschriften

Amyloid Formation

P. Chakraborty, S. Bera, P. Mickel, A. Paul, L. J. W. Shimon, Z. A. Arnon, D. Segal, P. Král*, E. Gazit* _____ **e202113845**

Inhibitor-Mediated Structural Transition in a Minimal Amyloid Model

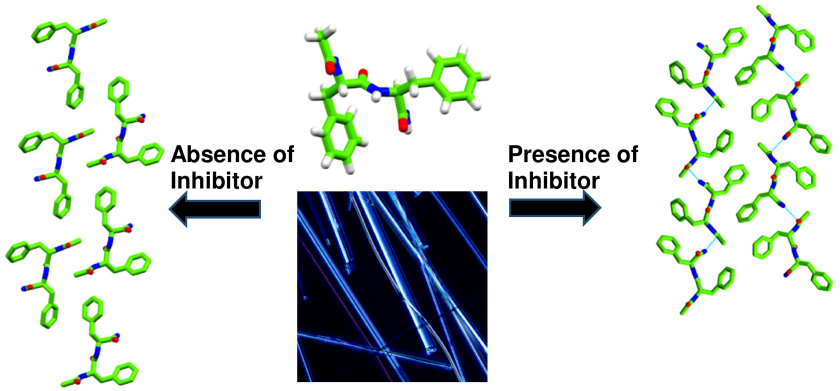

The crystal structure of the ultimate dipeptide that forms typical amyloid fibrils shows a canonical β-sheet structure at the atomic level. However, when crystallized in the presence of an amyloid-inhibitor the supramolecular packing of Ac-FF-NH_2 molecules rearranged into a supramolecular 2-fold helix (2_1 helix).